



Synthesis of magnetic biochar/carbonate intercalated Mg–Al layered double hydroxides for enhanced Cd(II) removal from aqueous solution

Qi Lv, Haixia Wang*, Mingliang Zhang, Junbing Xue, Jie Yang

School of Water Conservancy and Environment, University of Jinan, Jinan 250022, China, email: stu_wanghx@ujn.edu.cn (H. Wang)

Received 17 March 2020; Accepted 3 August 2020

ABSTRACT

Magnetic wheat straw biochar/Mg–Al layered double hydroxides (LDH) composites were prepared for Cd(II) removal from aqueous solution, and the adsorption performance and mechanisms were investigated. The results showed that magnetic biochar/carbonate intercalated Mg–Al LDH (MB/LDH-CO₃²⁻) exhibited excellent performance for Cd(II) removal, evidenced by the order of maximum removal capacities (MB/LDH-CO₃²⁻ (54.14 mg/g) > LDH-CO₃²⁻ (39.03 mg/g) > MB/LDH (35.25 mg/g) > LDH (27.65 mg/g) > BC (14.50 mg/g)). Carbonate anion intercalation with LDH increased the Cd(II) adsorption capacity, and decorating LDH-CO₃²⁻ with biochar further improved the adsorption performance because of the biochar internal space supplying a large reactive area. Based on X-ray diffraction and Fourier-transform infrared spectroscopy analyses, the adsorption mechanisms on Cd(II) efficient removal by MB/LDH-CO₃²⁻ were precipitation of CdCO₃, surface adsorption, surface complexation, and isomorphic substitution of Mg(II). Magnetic composites also improved the efficiency of separation from suspension after Cd(II) adsorption using a magnet. The results suggested that MB/LDH-CO₃²⁻ could be served as a potential material for efficient removal of Cd(II) from aqueous solution.

Keywords: Adsorption; Heavy metal; Biochar; Layered double hydroxides; Mechanism; Synergistic effect

1. Introduction

The toxicity of heavy metals has caused increasing public concern because of the widespread presence of heavy metals in industrial wastewater [1]. Cadmium (Cd) is considered as one of the most toxic heavy metals in aqueous solution or wastewater, due to its non-biodegradability, long biological half-life, and high biology accumulation. Long-time exposure on Cd can cause severe damage to human health. Therefore, it is urgent and essential to remove Cd(II) from aqueous solution or wastewater [2,3]. Various technologies have been developed for the decontamination of heavy metals, such as ion exchange, chemical method, membrane separation, reverse osmosis, and adsorption [4–6]. Adsorption is considered as one of the most promising

technologies because of its advantages of low cost, high efficiency, and flexible adjustment performance [7]. Various adsorbents have been used to adsorb Cd(II), such as activated carbon [8], biochar [9], zeolites [10], clay minerals [11], and so on. However, their large-scale use is very limited because of the difficulty in dispersing the powder adsorbent and low efficiency alone [12]. In view of these problems, combining magnetic, low cost, and high efficiency materials may improve the adsorption performance of Cd(II) [13].

Layered double hydroxides (LDH) is one type of anionic minerals with electropositive host layers and electro-negative intercalated anions, which can be used in adsorption, catalysis, nanotechnology and biotechnology, and other fields [14,15]. The excellent characteristics of LDHs (such as large specific surface areas, more active sites, and

* Corresponding author.

high temperature resistance) made it more beneficial to remove heavy metals [16]. Sun et al. [17] reported that LDH exhibited high adsorption ability for Cd(II) and the possible mechanisms were precipitation and complex formation. In addition, interlayer anion exchangeability is an important property of LDH. Various anions including organic and inorganic anions can be introduced into the LDHs layer, which can have influence on the performance of heavy metal removal. Mallakpour and Hatami [18] confirmed that raw LDH had relatively poor adsorption efficiency for Cd(II), while it was significantly improved after organic diacid intercalation modification. Zhang et al. [14] used L-cysteine to intercalate Mg–Al LDH, and the adsorption capacity of Cd(II) increased from 18.25 to 93.11 mg/g. Parida and Mohapatra [19] prepared Zn/Fe LDH with different intercalated anions (NO_3^- , Cl^- , and CO_3^{2-}) for photo degradation of azo dyes, and found that carbonate intercalated Zn/Fe LDH showed the highest activity. These studies showed that the intercalation method improved the adsorption performance of LDH. However, no systematic study was available on the effect of Cd(II) adsorption using LDH with carbonate anion intercalation.

Considering tight layer stacking for granular/bulk LDH may limit adsorption performance, the adsorption capacity of Cd(II) could be enhanced if an matrix was used to support LDH flakes and supply a large reactive area [20,21]. Biochar, a carbon-rich material derived from biomass pyrolysis in an oxygen-free environment, has been widely applied for wastewater treatment, soil improvement, and climate change mitigation [22–24]. Biochar also exhibited the advantage as good supporting material, due to abundant functional groups and surface charges, huge specific surface areas, and high stability [16,22]. Wang et al. [25] prepared biochar/Mn–Al LDH composites for Cu(II) removal from aqueous solution, and showed high sorption performance. However, the interactive effect between biochar and Mn–Al LDH was not extensively explored. Few studies focus on the synergistic effect between biochar and carbonate intercalated Mg–Al LDH for enhanced Cd(II) removal. In addition, the adsorption mechanism of biochar/carbonate intercalated LDHs composites on Cd(II) are also needed to be revealed.

Furthermore, the adsorbents applied for heavy metal removal are usually powders, which is difficult to separate the solid from a suspension after adsorption. In recent years, magnetic separation technology has attracted much attention to improve separation efficiency. Magnetic separation avoids time-consuming steps such as centrifugation and filtration, enabling fast solid–liquid separation [26,27]. Thus, in this study, magnetic biochar was produced by magnetite (Fe_3O_4) precipitation onto the surface of raw biochar, in order to permit simple separation by a magnetic field.

In this study, magnetic wheat straw biochar/Mg–Al LDH composites were synthesized by co-precipitation method for enhanced Cd(II) removal from aqueous solution. Adsorption batch experiment was performed to explore the effect of LDH with different anions intercalation on Cd(II) adsorption, and the synergistic effect of magnetic biochar and LDH on the performance of adsorption. The possible mechanisms of Cd(II) adsorption onto the composites were discussed in detail.

2. Materials and methods

2.1. Chemicals

Wheat straw samples were obtained from a farmland in Shandong province, China. All chemicals were of analytical grade, including aluminum chloride hexahydrate ($\text{AlCl}_3 \cdot 6\text{H}_2\text{O}$), magnesium chloride hexahydrate ($\text{MgCl}_2 \cdot 6\text{H}_2\text{O}$), sodium hydroxide (NaOH), nitric acid (HNO_3), ferric chloride ($\text{FeCl}_3 \cdot 6\text{H}_2\text{O}$), ferrous sulfate heptahydrate ($\text{FeSO}_4 \cdot 7\text{H}_2\text{O}$), sodium carbonate (Na_2CO_3), cadmium nitrate tetrahydrate ($\text{Cd}(\text{NO}_3)_2 \cdot 4\text{H}_2\text{O}$).

2.2. Preparation of biochar, LDH, and biochar/LDH composites

The wheat straw samples were washed with deionized water, and dried by oven at 80°C for 12 h. The dried biomass was smashed into powder with a pulverizer, and then sieved through a 0.3 mm sieve. The wheat straw biochar (BC) was derived from biomass pyrolysis at 600°C for 2 h under oxygen-free environment. Magnetic wheat straw biochar (MB) was prepared according to the method described by Karunanayake et al. [26]. Briefly, 5 g biochar were added into mixture solution (100 mL) containing 5.41 g $\text{FeCl}_3 \cdot 6\text{H}_2\text{O}$ and 2.78 g $\text{FeSO}_4 \cdot 7\text{H}_2\text{O}$, and stirred for 0.5 h. Then the mixture solution pH was adjusted to 10.5 by dropwise adding NaOH solution and stirred for 1 h. The obtained solid (MB) was washed with deionized water and then dried at 80°C overnight.

For the synthesis process of MB/LDH- CO_3^{2-} , then 25.4125 g $\text{MgCl}_2 \cdot 6\text{H}_2\text{O}$ and 15.0894 g $\text{AlCl}_3 \cdot 6\text{H}_2\text{O}$ ($\text{Mg}^{2+}/\text{Al}^{3+}$ molar ratio 2:1) were gradually dispersed in 100 mL deionized water, and 5 g magnetic biochar were mixed into the solution. Then the pH of the above solution was adjusted to 10.5 by dropwise adding the mixed alkaline solutions of NaOH and Na_2CO_3 (CO_3^{2-} intercalation). The resulting suspension was sealed and aged at 80°C for 12 h, and then the solid was washed with deionized water and dried at 80°C . Finally, the solid was sieved through a 0.1 mm sieve and yielded the MB/LDH- CO_3^{2-} . The synthesis process of LDH- CO_3^{2-} was same with MB/LDH- CO_3^{2-} except for without adding magnetic biochar. For LDH, the process was same with LDH- CO_3^{2-} except for the mixture solution pH being adjusted with NaOH and HNO_3 (NO_3^- intercalation). For MB/LDH, the process was same with MB/LDH- CO_3^{2-} except for the solution pH adjusted with NaOH and HNO_3 .

2.3. Characterization of materials

The X-ray diffraction (XRD) patterns of the materials before and after Cd(II) adsorption were obtained by D8 advance X-ray diffractometer (Bruker, Germany). The Brunauer–Emmett–Teller (BET) specific surface area, pore volume, and pore size was confirmed by a surface and porosity analyzer (ASAP 2020, Micromeritics, USA). The surface functional groups before and after adsorption were confirmed by Fourier-transform infrared spectroscopy (FTIR) spectrometer (FTS-165, PerkinElmer, United States) in the $400\text{--}4,000\text{ cm}^{-1}$ range. The micro-morphology structure and element distribution of the materials were obtained by scanning electron microscopy (SEM) and energy dispersive spectroscopy EDS (FEI Quanta FEG 250, FEI, USA).

The magnetic properties of the materials were investigated at 300 K using a 7404 vibrating sample magnetometer (VSM) (Lake Shore Cryotronics Inc., USA).

2.4. Adsorption procedure

A series of batch adsorption experiments were conducted to test the Cd(II) adsorption properties of MB/LDH-CO₃²⁻, MB/LDH, LDH-CO₃²⁻, LDH and BC, and reveal the effects of factors such as solution pH, reaction temperature, contact time, and adsorption isotherms (Table 1). All the experiments were carried out in duplicate (except for the experiment on adsorption comparison for different materials conducted in triplicate). The adsorption tests were performed in 100 mL plastic bottles with a certain amount of adsorbents and 25 mL of Cd(II) solution without shaking. The suspension was filtered immediately after the reaction, and the concentration of Cd(II) was analyzed by an AA-7000 atomic absorption spectrophotometer from Shimadzu Corporation, Japan. The wavelength was set at 228.8 nm resonance line and the slit width was 0.7 nm, and the measurements were carried out in an air/acetylene flame. The coefficient of correlation (*R*²) for calibration curve was larger than 0.999 and the recovery rate of blank spike was controlled in the range of 90%–110%.

2.5. Adsorption model fitting

The Langmuir and Freundlich models were used to analyze Cd(II) adsorption process by the materials. The linear equations are as follows:

$$\log q_e = \frac{1}{n} \log C_e + \log K_f \quad (1)$$

$$\frac{C_e}{q_e} = \frac{1}{K_L q_m} + \frac{C_e}{q_m} \quad (2)$$

where *C_e* (mg/L) is the equilibrium Cd(II) concentration, *q_e* (mg/g) is the equilibrium sorption amount, *q_m* (mg/g) is the maximum adsorption amount, *K_f* [(mg/g)/(mg/L)^{*n*}] and *K_L* (L/mg) are the constant of Freundlich and Langmuir model adsorption isothermal equation, respectively. *n* is the Freundlich constant related to the adsorption strength.

In order to evaluate the adsorption kinetics and diffusion mechanisms of Cd(II) onto MB/LDH-CO₃²⁻, MB/LDH, LDH-CO₃²⁻, LDH, and BC. The pseudo-first-order,

pseudo-second-order, and intraparticle diffusion models were used to fit the adsorption data. The fitting equations are described as follows:

$$\log(q_e - q_t) = \log q_e - \frac{K_1 t}{2.303} \quad (3)$$

$$\frac{t}{q_t} = \frac{1}{K_2 q_e^2} + \frac{t}{q_e} \quad (4)$$

$$q_t = K_p t^{1/2} + C \quad (5)$$

where *K₁* (1/min), *K₂* (g/(mg min)), and *K_p* are the rate constants of pseudo-first-order, pseudo-second-order, and intraparticle diffusion model, respectively. *q_t* and *q_e* (mg/g) are the Cd(II) amounts adsorbed by the materials at time and equilibrium, respectively. *C* is a constant related to the thickness of the boundary layer.

3. Results and discussion

3.1. Characterization of adsorbents

3.1.1. XRD analysis

Fig. 1 shows the XRD patterns of MB/LDH-CO₃²⁻, MB/LDH, LDH-CO₃²⁻, LDH, and BC. The characteristic peaks at 2θ values of 11.6°, 23.3°, 34.8°, 39.3°, 46.7°, 60.8°, and 62.1° were assigned to the (003), (006), (012), (015), (018), (110), and (113) planes of Mg–Al LDH, respectively [28]. The sharp diffraction peaks indicated that the Mg–Al LDH with high crystallinity was produced [25]. The peak intensity of MB/LDH-CO₃²⁻ and MB/LDH weakened, indicating that the purity and crystallinity materials were reduced due to LDH particles loading on biochar. However, there were no significant changes in the positions of the seven representative diffraction peaks after the modification of LDH, and the characteristic diffraction peaks of MB/LDH-CO₃²⁻ or MB/LDH were all corresponded to the characteristic peaks of Mg–Al LDH, indicating that carbonate intercalation and magnetic biochar loading did not much change the crystallinity structure of LDH. The (012), (015), (018), and (110) characteristic diffraction peaks of MB/LDH-CO₃²⁻ and LDH-CO₃²⁻ were sharper, indicating that carbonate ions were successfully inserted between the Mg–Al LDH layers, forming a hexagonal lattice structure [27]. According to Bragg's law ($2d\sin\theta = n\lambda$), the basal spacing *d*₀₀₃ of LDH

Table 1
Experimental conditions of Cd(II) adsorption

Experiment	Dosage (g/L)	Concentration (mg/L)	Solution volume (mL)	Solution pH	Contact time (h)	Temperature (°C)
Effect of solution pH	2	50	25	3–7	24	25
Effect of contact time	2	50	250	6	0.08–72	25
Adsorption isotherm	2	25–250	25	6	24	25
Effect of temperature	2	50	25	6	24	4–45
Comparison for adsorption ability	2	100	25	6	24	25

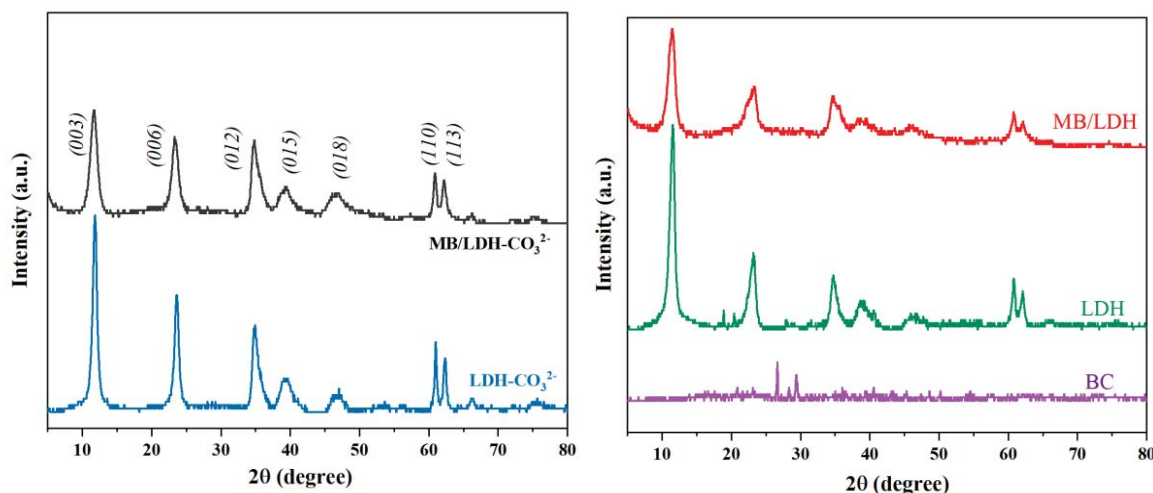


Fig. 1. XRD patterns of MB/LDH-CO₃²⁻, MB/LDH, LDH-CO₃²⁻, LDH, and BC.

was 0.76 nm, and d_{006} was 0.38 nm. In addition, the basal spacing d_{003} of MB/LDH-CO₃²⁻ was 0.75 nm, and d_{006} was 0.38 nm. It indicated that the materials had good-layered structure and high crystallinity [29].

3.1.2. FTIR analysis

The FTIR spectra of MB/LDH-CO₃²⁻, MB/LDH, LDH-CO₃²⁻, LDH, and BC are shown in Fig. 2. For LDH-CO₃²⁻ and MB/LDH-CO₃²⁻, the broad adsorption peaks at around 1,360 and 787 cm⁻¹ can be attributed to the tensile/bending vibration mode of the CO₃²⁻ anion interposed between the LDH plates. The peaks at 1,640 and 3,450 cm⁻¹ corresponded to tensile and flexural vibrations of hydroxyl groups and H₂O molecules [30]. The peaks at 450–800 cm⁻¹, including 557, 669, and 450 cm⁻¹, were assigned to Al–O or Mg–O band tensile vibration, which proved that the metal ions in the laminate were mainly Mg and Al [31]. For MB/LDH and LDH, the absorption peaks at around 1,370 cm⁻¹ corresponds to the antisymmetric stretching of the NO₃⁻ present in LDH plates [17]. The small peaks of MB/LDH-CO₃²⁻ and MB/LDH at 860 cm⁻¹ were caused by aromatic C–H bending vibration which may favor for Cd(II) adsorption, such as forming complexes with aromatic C–H [32]. All the characteristic peaks of the composites were similar to the characteristic peaks of LDH, which proved that neither carbonate intercalation nor the supported magnetic biochar changed the crystal structure of LDH.

3.1.3. SEM and EDS analysis

Micro-morphology and elemental composition of the prepared materials are shown in Fig. 3. The surface and inner wall of the biochar were uniformly covered by LDH-CO₃²⁻ or LDH (Figs. 4a and b). The difference was that the LDH surfaces after carbonate intercalation were more complicated and rough, probably due to a larger specific surface area and complex pore structures for MB/LDH-CO₃²⁻. Evenly distribution of LDH-CO₃²⁻ particles on the biochar can alleviate the aggregation of powder particles, which

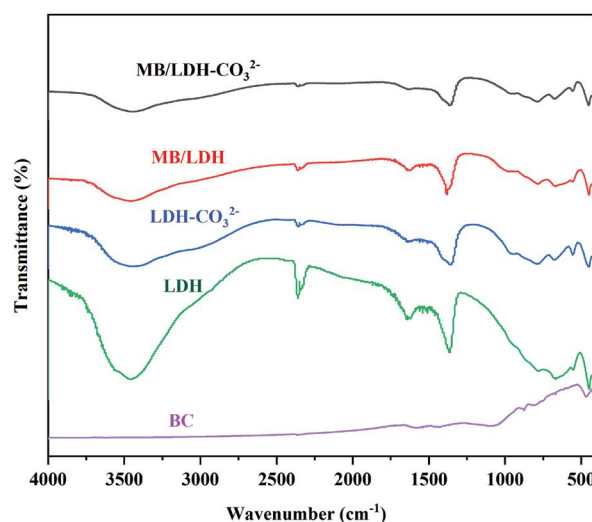


Fig. 2. FTIR spectra of MB/LDH-CO₃²⁻, MB/LDH, LDH-CO₃²⁻, LDH, and BC.

can supply a large reactive area to improve the adsorption performance. As seen from Table 2, the carbon content of LDH was significantly increased after carbonate intercalation, while chloride ions decreased to below detection. This result was consistent with the speculation that carbonates intercalated in the interlayer [29]. The carbon atomic percentages of MB/LDH-CO₃²⁻, MB/LDH, BC, LDH-CO₃²⁻, LDH were 83.74%, 75.91%, 76.44%, 5.37%, and 2.61%, respectively. Therefore, magnetic biochar was well combined with LDH, and LDH may be more conducive to Cd(II) adsorption after carbonate intercalation.

3.1.4. BET analysis

The pore structures of the material were also characterized by the BET method (Table 2). After carbonate intercalation, the specific surface area of LDH increased from 55.20 to 98.01 m²/g, and the pore volume and pore

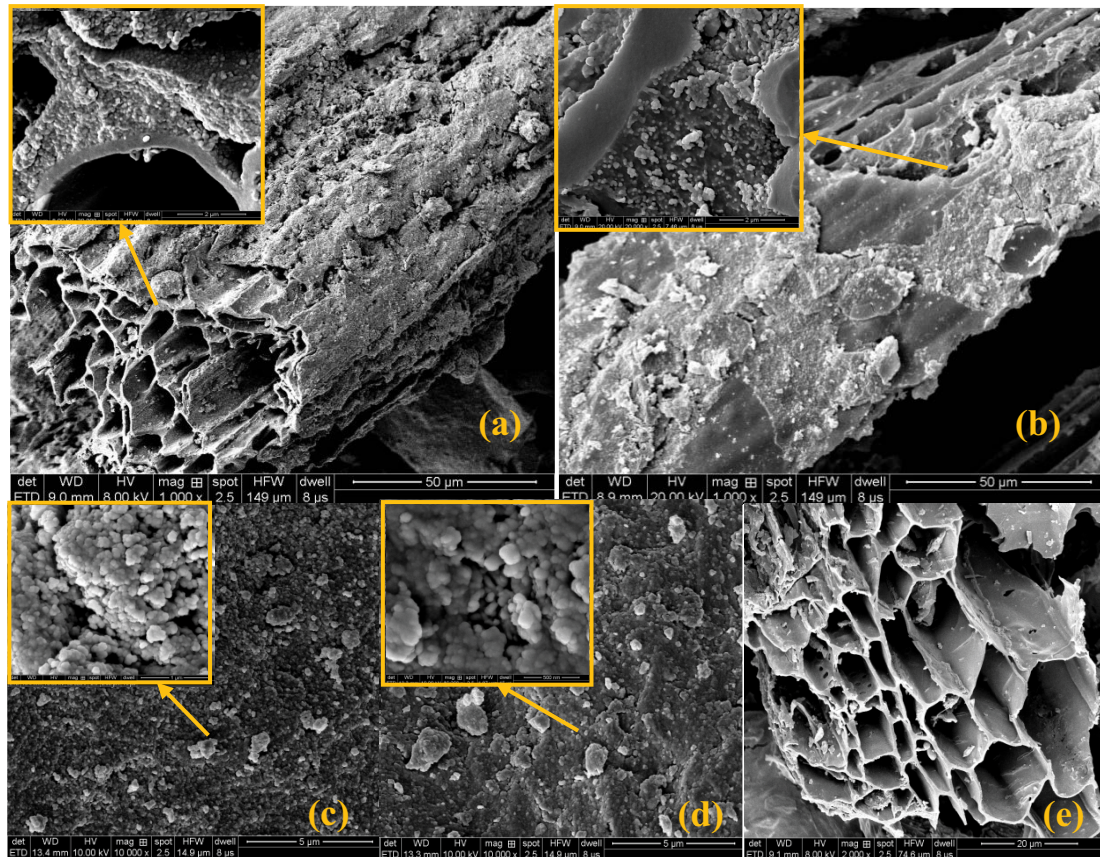


Fig. 3. SEM images of MB/LDH-CO₃²⁻ (a), MB/LDH (b), LDH-CO₃²⁻ (c), LDH (d), and BC (e).

Table 2
Elemental composition and BET analysis results of the materials

Materials	Atomic ratio (%)					BET surface area (m ² /g)	Pore volume (cm ³ /g)	Pore diameter (nm)	Basal spacing (nm)	
	C	Fe	Mg	Al	Cl				<i>d</i> ₀₀₃	<i>d</i> ₀₀₆
MB/LDH-CO ₃ ²⁻	83.74	0.08	0.43	0.17	N	123.15	0.44	14.36	0.75	0.38
MB/LDH	75.91	0.33	0.90	0.37	0.30	73.07	0.17	9.44	0.77	0.38
LDH-CO ₃ ²⁻	5.37	N	17.18	8.09	N	98.01	0.51	20.70	0.75	0.38
LDH	2.61	N	11.33	12.45	2.61	55.20	0.16	11.29	0.76	0.38
BC	76.44	N	0.10	N	0.06	97.87	0.07	2.90	/	/

N: No detection.

diameter increased. After loaded onto the magnetic biochar, the specific surface area of MB/LDH-CO₃²⁻ further increased to 123.15 m²/g. This result indicated that the insertion of carbonates increased the specific surface area, pore volume, and pore size, which was consistent with the SEM image. In addition, the larger specific surface area of materials, the more active sites might be provided. Thus, it may be more conducive for Cd(II) adsorption onto MB/LDH-CO₃²⁻.

3.1.5. Magnetization analysis

The saturation magnetization of MB/LDH-CO₃²⁻ and MB/LDH was 1.8 and 2.8 emu/g at 300 K (27°C), respectively

(Fig. 5). The two materials exhibited magnetic behavior and could be readily attracted by magnet after use, although they are relatively weak.

3.2. Influence factors on the Cd(II) adsorption

Optimal conditions for Cd(II) adsorption, such as reaction temperature, solution pH, contact time, and Cd(II) initial concentration were shown in Fig. 6. The adsorption of Cd(II) on all materials was significantly affected by solution pH (Fig. 6a). As the pH of the solution increased, the adsorption capacity gradually increased. In the lower pH environment, functional groups such as -OH and -COO on the surface of the adsorbent are protonated, which

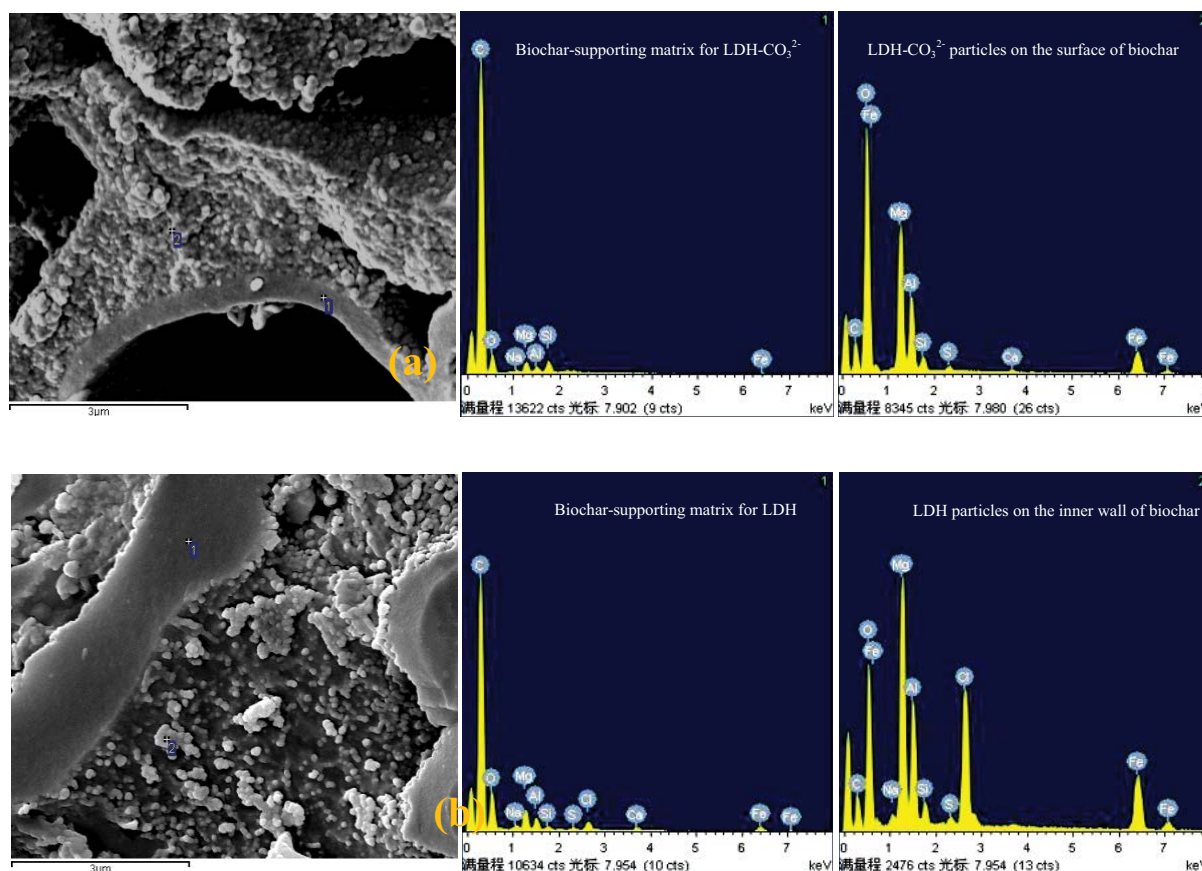


Fig. 4. EDS images of MB/LDH-CO₃²⁻ (a) and MB/LDH (b).

will cause electrostatic repulsion with Cd(II). Increasing pH deprotonates surface functional groups and leads to more negatively charged adsorption sites and Cd(II) was adsorbed on the surface of the adsorbent due to electrostatic attraction [26].

The effect of adsorption time on the adsorption capacity of materials is shown in Fig. 6c. The removal ratio of Cd(II) sharply increased in the first 10 h, and it slowed down gradually afterwards. In the early stage of adsorption, the adsorption rate was fast because of abundant adsorption active sites. With the passage of time, the active sites on the materials surface decreased, and the Cd(II) concentration in the solution also slowly decreased, resulting in a slower adsorption rate. Fig. 6b shows the effect of temperature on Cd(II) adsorption onto MB/LDH-CO₃²⁻, MB/LDH, LDH-CO₃²⁻, and LDH. The temperature increased, the removal rate of Cd(II) by materials increased, which might indicate that the adsorption process was slightly endothermic, or increasing temperature would increase the diffusion rate of Cd(II) into the micropores. This showed that temperature had an effect on the adsorption of Cd(II) by materials, and proper heating was favorable for Cd(II) adsorption [9,26].

As the concentration of Cd(II) in the solution increased, the adsorption capacity gradually increased, and reached equilibrium at a high concentration of 200–250 mg/L (Fig. 6d). As can be seen from Fig. 6e, at the initial concentration of Cd(II) 100 mg/L, the removal efficiency was 39.97%,

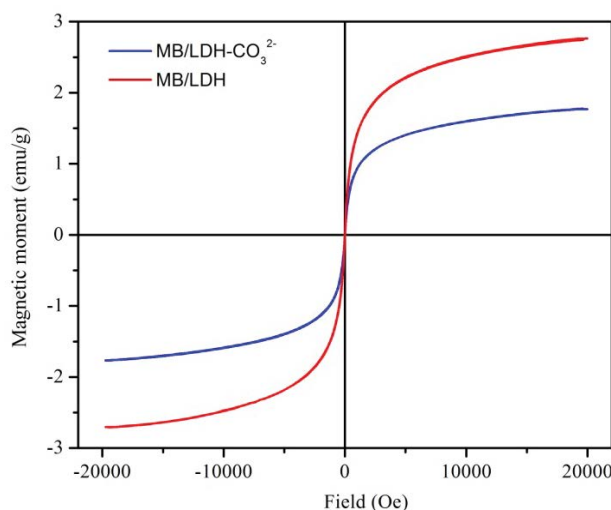


Fig. 5. Magnetic moment of MB/LDH-CO₃²⁻ and MB/LDH at 300 K.

29.31%, 37.75%, 22.52%, and 12.76% for MB/LDH-CO₃²⁻, LDH-CO₃²⁻, MB/LDH, LDH, and BC, respectively. It indicated that carbonate intercalation with LDH improved the ability to remove Cd(II), and loading magnetic biochar further improved the removal efficiency.

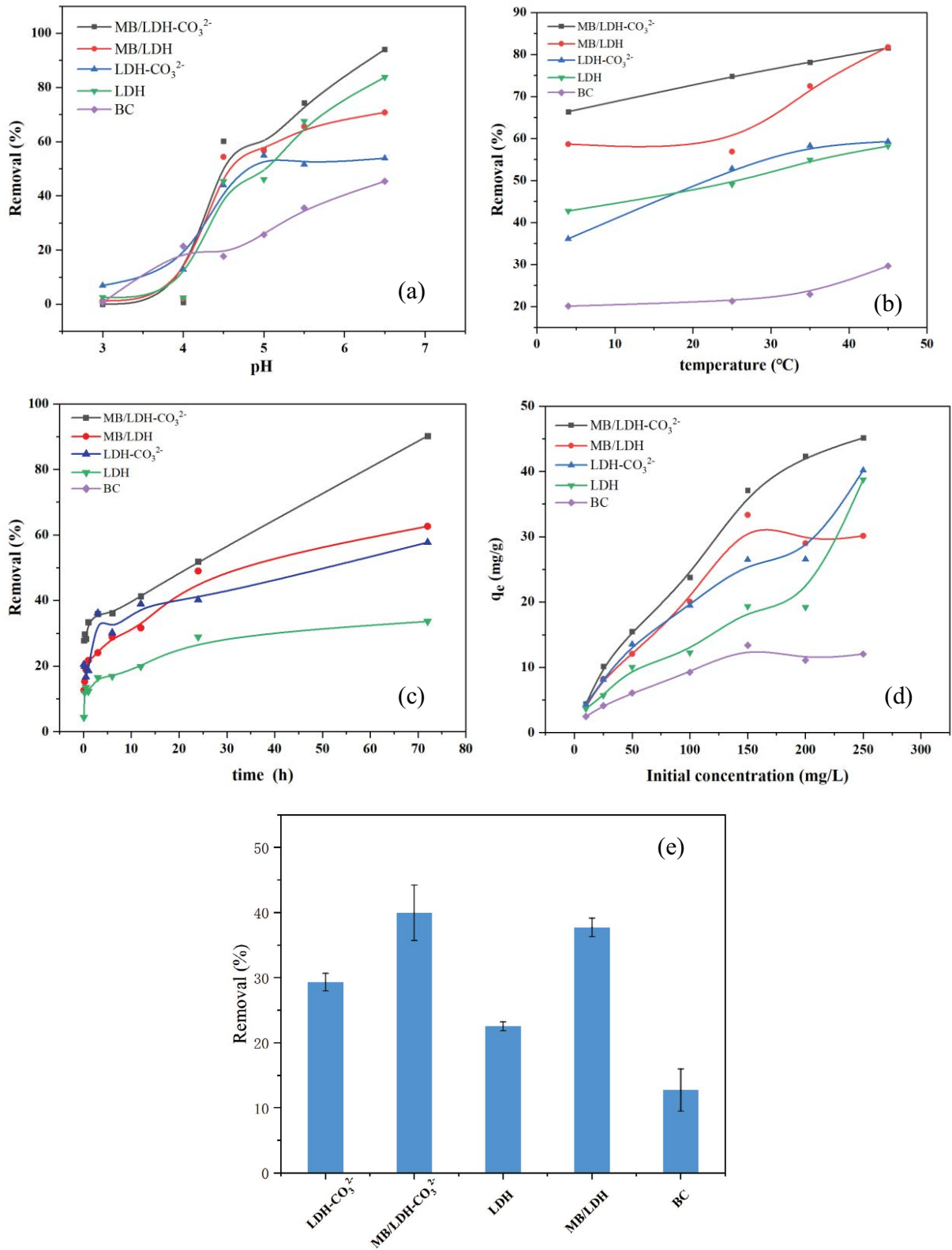


Fig. 6. Effect of solution pH (a), reaction temperature (b), contact time (c), Cd(II) initial concentration (d), and adsorption comparison for different materials (e).

3.3. Adsorption isotherms

The parameters of the Langmuir and Freundlich isotherm models are shown in Table 3. The adsorption data fits the Langmuir better than Freundlich model, especially for MB/LDH-CO₃²⁻ (Fig. 7). This indicated that the adsorption of Cd(II) by the material was monolayer adsorption [14]. The maximum adsorption capacity (q_m) was calculated based on the Langmuir isotherm equation: MB/LDH-CO₃²⁻ (54.14 mg/g) > LDH-CO₃²⁻ (39.03 mg/g) > MB/LDH (35.25 mg/g) > LDH (27.65 mg/g) > BC (14.50 mg/g). It was clear that the carbonate intercalation LDH improved the ability to remove Cd(II), and further improved after loading magnetic biochar due to their synergistic effect. Combined with the characterization results, carbonate intercalation with LDH provided another mechanism to remove Cd(II), and magnetic biochar brought the greater specific surface area to supply more reactive sites. The Langmuir parameter ($1/n$) ranging from zero to one indicates the adsorption is favorable [33]. The value of n for Cd (II) adsorption on biochar/ LDH showed that Cd(II) was easily absorbed. The separation factor (R_L) of the Langmuir isotherm model is defined as $R_L = 1/(1 + K_L C_0)$, where C_0 is the initial Cd(II) concentration. The value of R_L for MB/

LDH-CO₃²⁻ less than 1 indicated Cd(II) adsorption was favorable [34]. Table 4 shows that the maximum adsorption capacity of Cd(II) onto MB/LDH-CO₃²⁻ is comparable with other adsorbents reported in the literature.

3.4. Adsorption kinetics

The parameters of adsorption kinetics are shown in Table 5. The correlation coefficient of the pseudo-second-order model ($R^2 > 0.93$) exceeded that of the pseudo-first-order model ($R^2 > 0.69$), and the calculated adsorption amounts ($q_{e,cal}$) were consistent with the experimental adsorption amounts ($q_{e,exp}$). The adsorption data fit the pseudo-second-order model well. This indicated that the adsorption rate of Cd(II) by materials was mainly controlled by chemical reactions [17]. The bonding between active sites (e.g., CO₃²⁻, -OH) and Cd(II) might dominate the adsorption rate, consisting with Mallakpour and Hatami [18] previous reports.

The intraparticle diffusion model further explained the diffusion mechanisms of Cd(II). None of the fitted straight lines passed through the origin, which indicated that the adsorption diffusion processes were affected by multiple diffusion mechanisms [43]. The fitted graphs were presented in two stages, so the diffusion mechanisms of Cd(II)

Table 3
Langmuir and Freundlich model parameters obtained for Cd(II) adsorption

Materials	Freundlich model			Langmuir model		
	K_f (mg/g)/(mg/L) ⁿ	1/n	R^2	q_m (mg/g)	K_L (L/mg)	R^2
MB/LDH-CO ₃ ²⁻	4.92	0.45	0.97	54.14	0.03	0.91
MB/LDH	3.27	0.45	0.95	35.25	0.04	0.96
LDH-CO ₃ ²⁻	4.31	0.39	0.93	39.03	0.03	0.86
LDH	2.63	0.42	0.80	27.65	0.02	0.70
BC	1.23	0.45	0.96	14.50	0.03	0.96

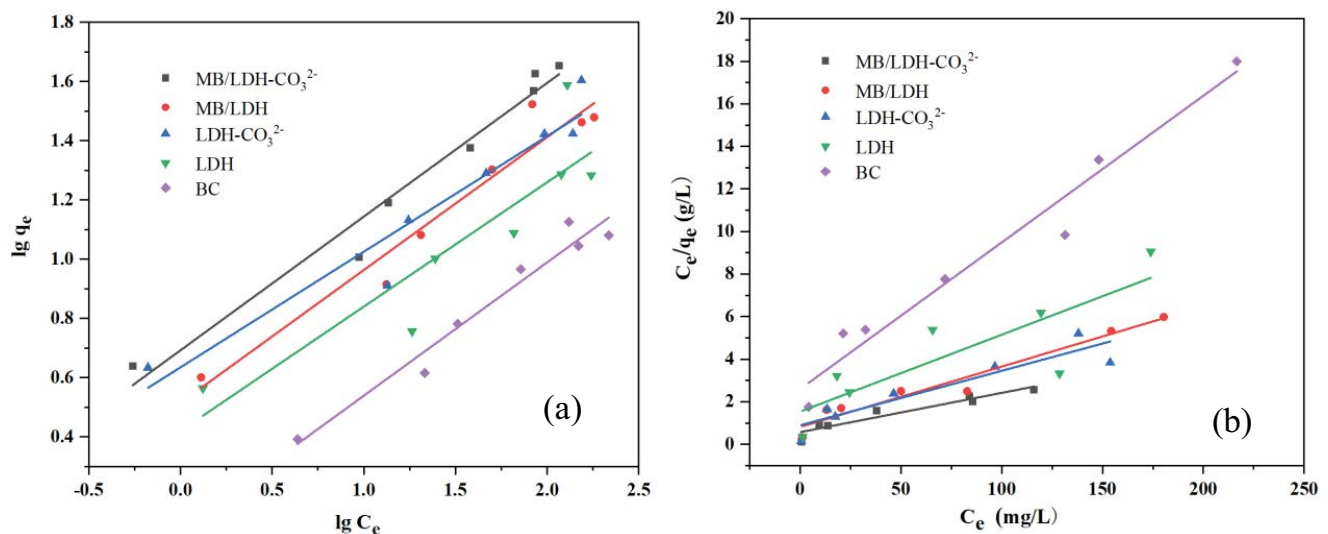


Fig. 7. Linear Freundlich (a) and Langmuir (b) isotherm of Cd(II) adsorption onto the adsorbents.

Table 4
Removal capacities of Cd(II) on MB/LDH-CO₃²⁻ compared with other materials

Materials	Temperature (°C)	pH	q _e (mg/g)	References
Carbon nanotubes	45	8	25.70	[35]
EDTA-LDH/PVA NC 8%	25	5	9.54	[36]
Chitosan-pyromellitic dianhydride modified biochar	35	5	38.24	[37]
Dashukivskij bentonite	25	7	26.04	[38]
Nanosized Fe ₃ O ₄ /bentonite nanocomposites	25	-	21.70	[39]
Modified fly ash	25	6	56.31	[40]
Mesoporous silica nanospheres	30	5	32.98	[41]
Chitosan modified with complexation	25	3	38.50	[42]
MB/LDH-CO ₃ ²⁻	25	6	54.14	This work

Table 5
Calculated parameters of kinetic models for the adsorption of Cd(II) on the materials

Models	Parameters	Units	MB/LDH-CO ₃ ²⁻	MB/LDH	LDH-CO ₃ ²⁻	LDH
Pseudo-first-order	q _{e,exp}	mg/g	20.77	14.43	13.29	7.74
	q _{e,cal}	mg/g	13.90	10.76	8.06	5.44
	K ₁	1/min	21.00	0.0008	0.0006	0.0010
	R ²		0.96	0.96	0.69	0.93
Pseudo-second-order	q _{e,cal}	mg/g	20.67	14.74	13.29	7.89
	K ₂	g/(mg min)	0.0002	0.0003	0.0004	0.0007
	R ²		0.93	0.97	0.98	0.99
	K _{p1}	mg/(g min ^{1/2})	0.17	0.39	0.34	0.19
Intraparticle diffusion	C ₁		6.01	2.06	2.94	1.43
	R ²		0.87	0.99	0.66	0.65
	K _{p2}	mg/(g min ^{1/2})	0.27	0.18	0.13	0.08
	C ₂		2.44	3.32	4.85	2.62
	R ²		0.98	0.96	0.96	0.89

in materials were: (1) Cd(II) penetrated the liquid film and quickly spread to the surfaces of the materials; (2) Cd(II) diffused into the pores after entering the materials. It was clear that the K_{p1} of MB/LDH-CO₃²⁻ was larger, which might be attributed to the large specific surface area that could receive more Cd(II) to assist the chemisorption.

3.5. Adsorption mechanisms

Isotherms and kinetic analysis showed that the adsorption mechanism of Cd(II) by MB/LDH-CO₃²⁻ might involved chemisorption and bonding. To further elucidate the Cd(II) adsorption mechanisms, XRD and FTIR analyses of the adsorbents were conducted.

The XRD patterns of the MB/LDH-CO₃²⁻, MB/LDH, LDH-CO₃²⁻, and LDH before and after adsorption of Cd(II) are shown in Fig. 8. It was clear that the peaks of (012), (015), (018), and (110) for MB/LDH-CO₃²⁻ and LDH-CO₃²⁻ almost disappeared after Cd(II) adsorption. Meanwhile, four new peaks at 2θ were 30.42°, 36.25°, 43.64°, and 49.90° for MB/LDH-CO₃²⁻ and LDH-CO₃²⁻ appeared (Fig. 8), which belong to the typical diffractions of CdCO₃ [15]. This indicated that interlayer CO₃²⁻ participated in the adsorption

reaction, and the precipitated CdCO₃ accumulated in the LDH layer [44]. In addition, the seven peaks for MB/LDH-CO₃²⁻ were significantly weakened or disappeared after Cd(II) adsorption, which might be due to the collapse of the crystal structure caused by MB/LDH-CO₃²⁻ adsorbing too much Cd(II). While, no new peaks appeared in the patterns of MB/LDH and LDH after Cd(II) adsorption, indicating the formation of CdCO₃ precipitation was not the main adsorption mechanisms. The FTIR analysis (Fig. 9) showed that the band at around 1380 cm⁻¹ that emerged in LDH-CO₃²⁻ and MB/LDH-CO₃²⁻ after Cd(II) adsorption could be attributed to the band of CdCO₃ [15].

The crystal structure of LDH is similar to that of brucite, in which six OH⁻ ions surround each Mg(II) to form an octahedral structure and the different octahedral units share their edges to form infinite sheets [45]. Divalent metal cations in octahedral units of the hydroxide sheet can be easily replaced by other metal cations with similar ionic radius, through the process of isomorphous substitution. The ionic radius of Cd(II) (0.095 nm) was similar to that of Mg(II) (0.066 nm) [14], so Mg(II) on LDH laminates are extremely prone to be replaced by Cd(II) in solution. The isomorphous substitution was also proven by more released amount of

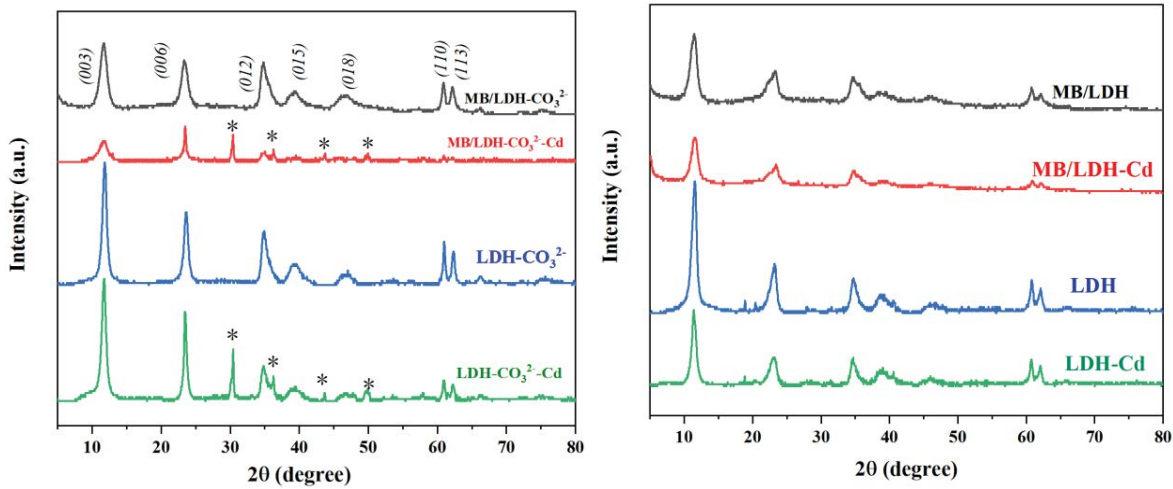


Fig. 8. XRD patterns of MB/LDH-CO₃²⁻, MB/LDH, LDH-CO₃²⁻ and LDH before and after Cd(II) adsorption (*peak of CdCO₃).

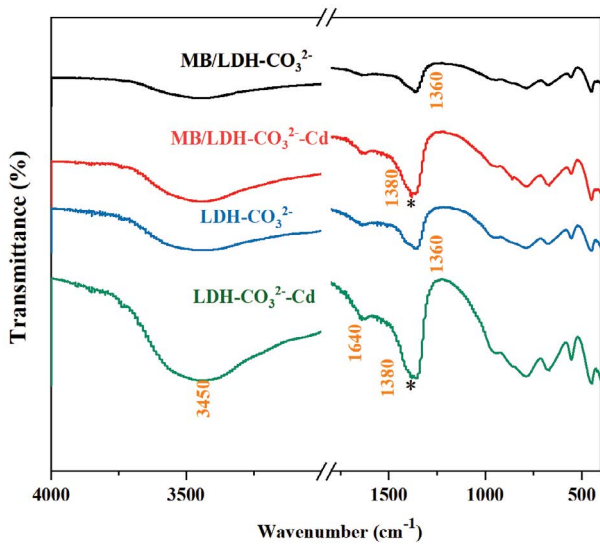


Fig. 9. FTIR spectra of MB/LDH-CO₃²⁻ and LDH-CO₃²⁻ before and after Cd(II) adsorption (*band of CdCO₃).

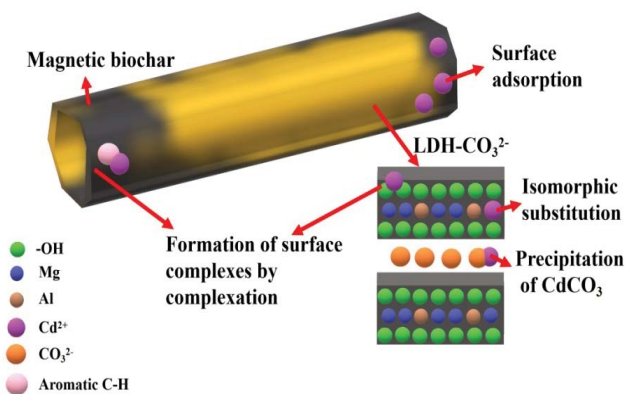


Fig. 10. Schematic diagram of adsorption mechanism of Cd(II) onto MB/LDH-CO₃²⁻.

Mg(II) was detected after Cd(II) adsorption in many studies. Similar isomorphous substitution in LDH crystal structure have also been reported in literature [25]. In addition, the formation of outer-sphere surface complexes (O-Cd) between Cd(II) and some deprotonated hydroxyl groups (O⁻) and surface adsorption derived from electrostatic attraction also contributed the adsorption of Cd(II) [17].

Therefore, the preferred mechanisms of Cd(II) adsorption by MB/LDH-CO₃²⁻ may include: (i) formation of CdCO₃ precipitation with interlayer CO₃²⁻, (ii) isomorphous substitution of Mg(II) with Cd(II), (iii) formation of surface complexes by complexation, and (iv) surface adsorption due to electrostatic effects (Fig. 10).

4. Conclusions

In this study, MB/LDH-CO₃²⁻ composites exhibited the enhanced adsorption capacity for Cd(II), due to the carbonate anion intercalation with LDH and large reactive matrix supported by biochar. The synergistic effect between biochar and carbonate intercalated LDH occurred for enhanced Cd(II) removal. The maximum adsorption capacity of Cd(II) by MB/LDH-CO₃²⁻ was 54.14 mg/g at pH 6. The main adsorption mechanism involved the precipitation of CdCO₃, surface adsorption, surface complexation, and isomorphous substitution of Mg(II). MB/LDH-CO₃²⁻ could be quickly separated from the solution by a magnet after adsorption. These findings showed that MB/LDH-CO₃²⁻ can be considered as an efficient adsorbent for Cd(II) removal from aqueous solution.

Acknowledgment

This research was funded by Doctoral Foundation of University of Jinan (XBS1920) and Natural Science Foundation of Shandong Province, China (ZR2018MEE007).

References

[1] H. Chen, Y. Meng, S. Jia, W. Hua, Y. Cheng, J. Lu, H. Wang, Graphene oxide modified waste newspaper for removal of

- heavy metal ions and its application in industrial wastewater, *Mater. Chem. Phys.*, 244 (2020) 122692, doi: 10.1016/j.matchemphys.2020.122692.
- [2] H.A. El-Azim, M.M. El-Sayed Seleman, E.M. Saad, Applicability of water-spray electric arc furnace steel slag for removal of Cd and Mn ions from aqueous solutions and industrial wastewaters, *J. Environ. Chem. Eng.*, 7 (2019), doi: 10.1016/j.jece.2019.102915.
- [3] H. Chen, L. Tang, Z. Wang, M. Su, D. Tian, L. Zhang, Z. Li, Evaluating the protection of bacteria from extreme Cd(II) stress by P-enriched biochar, *Environ. Pollut.*, 263 (2020), doi: 10.1016/j.envpol.2020.114483.
- [4] Y. Zhu, W.H. Fan, T.T. Zhou, X.M. Li, Removal of chelated heavy metals from aqueous solution: a review of current methods and mechanisms, *Sci. Total Environ.*, 678 (2019) 253–266.
- [5] S. Kim, K.H. Chu, Y.A. Al-Hamadani, C.M. Park, M. Jang, D.H. Kim, M. Yu, J. Heo, Y. Yoon, Removal of contaminants of emerging concern by membranes in water and wastewater: a review, *Chem. Eng. J.*, 335 (2018) 896–914.
- [6] M. Naushad, A. Mittal, M. Rathore, V. Gupta, Ion-exchange kinetic studies for Cd(II), Co(II), Cu(II), and Pb(II) metal ions over a composite cation exchanger, *Desal. Water Treat.*, 54 (2015) 2883–2890.
- [7] B. Dash, B. Dash, S.S. Arth, A thorough understanding of the adsorption of Ni(II), Cd(II) and Zn(II) on goethite using experiments and molecular dynamics simulation, *Sep. Purif. Technol.*, 240 (2020) 116649, doi: 10.1016/j.seppur.2020.116649.
- [8] W.L. Wang, Y. Liu, X.H. Liu, Equilibrium adsorption study of the adsorptive removal of Cd²⁺ and Cr⁶⁺ using activated carbon, *Environ. Sci. Pollut. Res.*, 25 (2018) 25538–25550, doi: 10.1007/s11356-018-2635-5.
- [9] R. Gao, H. Hu, Q. Fu, Z. Li, Z. Xing, U. Ali, Y. Liu, Remediation of Pb, Cd, and Cu contaminated soil by co-pyrolysis biochar derived from rape straw and orthophosphate: speciation transformation, risk evaluation and mechanism inquiry, *Sci. Total Environ.*, 730 (2020) 139119, doi: 10.1016/j.scitotenv.2020.139119.
- [10] J.Z. Lima, I.M. Raimondi, V. Rodrigues, Preliminary Study of the Adsorption Capacity of Pb, Zn and Cd Through Zeolite and Organic Compost, A. Shakoor, K. Cato, Eds., IAEG/AEG Annual Meeting Proceedings, San Francisco, CA, Vol. 3, Springer, Cham, 2018, pp. 27–33.
- [11] S.Q. Gu, X.N. Kang, L. Wang, Clay mineral adsorbents for heavy metal removal from wastewater: a review, *Environ. Chem. Lett.*, 17 (2019) 629–654.
- [12] Z.N. Syamimi, S. Johan, M. Khalida, Magnetic field application and its potential in water and wastewater treatment systems, *Sep. Purif. Rev.*, 43 (2014) 206–240.
- [13] K.R. Thines, E.C. Abdullah, N.M. Mubarak, M. Ruthiraan, Synthesis of magnetic biochar from agricultural waste biomass to enhancing route for waste water and polymer application: a review, *Renewable Sustainable Energy Rev.*, 67 (2017) 257–276.
- [14] X. Zhang, L.G. Yan, J. Li, H.Q. Yu, Adsorption of heavy metals by l-cysteine intercalated layered double hydroxide: kinetic, isothermal and mechanistic studies, *J. Colloid Interface Sci.*, 562 (2020) 149–158.
- [15] R.R. Shan, L.G. Yan, K. Yang, Y.F. Hao, B. Du, Adsorption of Cd(II) by Mg–Al–CO₃- and magnetic Fe₃O₄/Mg–Al–CO₃-layered double hydroxides: kinetic, isothermal, thermodynamic and mechanistic studies, *J. Hazard. Mater.*, 299 (2015) 42–49.
- [16] Z.R. Zhang, L.G. Yan, H.Q. Yu, T. Yan, G.X. Li, Adsorption of phosphate from aqueous solution by vegetable biochar/layered double oxides: fast removal and mechanistic studies, *Bioresour. Technol.*, 284 (2019) 65–71.
- [17] J.H. Sun, Y. Chen, H.Q. Yu, L.G. Yan, B. Du, Z.G. Pei, Removal of Cu²⁺, Cd²⁺ and Pb²⁺ from aqueous solutions by magnetic alginate microspheres based on Fe₃O₄/MgAl-layered double hydroxide, *J. Colloid Interface Sci.*, 532 (2018) 474–484.
- [18] S. Mallakpour, M. Hatami, Biosafe organic diacid intercalated LDH/PVC nanocomposites versus pure LDH and organic diacid intercalated LDH: synthesis, characterization and removal behaviour of Cd²⁺ from aqueous test solution, *Appl. Clay Sci.*, 149 (2017) 28–40.
- [19] K.M. Parida, L. Mohapatra, Carbonate intercalated Zn/Fe layered double hydroxide: a novel photocatalyst for the enhanced photo degradation of azo dyes, *Chem. Eng. J.*, 179 (2012) 131–139.
- [20] Y.Y. Wang, H.Y. Ji, H.H. Lyu, Y.X. Liu, L.L. He, L.C. You, C.H. Zhou, S.M. Yang, Simultaneous alleviation of Sb and Cd availability in contaminated soil and accumulation in *Lolium multiflorum* Lam. After amendment with Fe–Mn-Modified biochar, *J. Cleaner Prod.*, 231 (2019) 556–564.
- [21] M. Zubair, M. Daud, G. McKay, F. Shehzad, M.A. Al-Harathi, Recent progress in layered double hydroxides (LDH)-containing hybrids as adsorbents for water remediation, *Appl. Clay Sci.*, 143 (2017) 279–292.
- [22] P. Regmi, J.L. Garcia Moscoso, S. Kumar, X.Y. Cao, J.D. Mao, G. Schafran, Removal of copper and cadmium from aqueous solution using switchgrass biochar produced via hydrothermal carbonization process, *Environ. Manage.*, 109 (2012) 61–69.
- [23] M. Imran, Z.U.H. Khan, M.M. Iqbal, J. Iqbal, N.S. Shah, S. Munawar, M. Rizwan, Effect of biochar modified with magnetite nanoparticles and HNO₃ for efficient removal of Cr(VI) from contaminated water: a batch and column scale study, *Environ. Pollut.*, 261 (2020) 114231, doi: 10.1016/j.envpol.2020.114231.
- [24] A. Bagheri, E. Abu-Danso, J. Iqbal, A. Bhatnagar, Modified biochar from Moringa seed powder for the removal of diclofenac from aqueous solution, *Environ. Sci. Pollut. Res.*, 27 (2020) 7318–7327.
- [25] T. Wang, C. Li, C.Q. Wang, H. Wang, Biochar/MnAl-LDH composites for Cu(II) removal from aqueous solution, *Colloids Surf.*, A, 538 (2018) 438–450.
- [26] A.G. Karunanayake, O.A. Todd, M. Crowley, L. Ricchetti, C.U. Pittman, Lead and cadmium remediation using magnetized and nonmagnetized biochar from Douglas fir, *Chem. Eng. J.*, 331 (2018) 480–491.
- [27] J.L. Guimaraes, R. Marangoni, L.P. Ramos, F. Wypych, Covalent grafting of ethylene glycol into the Zn–Al–CO₃ layered double hydroxide, *J. Colloid Interface Sci.*, 227 (2000) 445–451.
- [28] G. Gao, Z. Zhu, J. Zheng, Z. Liu, Q. Wang, Y.S. Yan, Ultrathin magnetic Mg–Al LDH photocatalyst for enhanced CO₂ reduction: fabrication and mechanism, *J. Colloid Interface Sci.*, 555 (2019) 1–10.
- [29] Š. Paušová, J. Krýsa, J. Jirkovský, C. Forano, G. Mailhot, V. Prevot, Insight into the photocatalytic activity of ZnCr–CO₃ LDH and derived mixed oxides, *Appl. Catal., B*, 170–171 (2015) 25–33.
- [30] A.A. Sakr, T. Zaki, O. Elgabry, M.A. Ebiad, S.M. El-Sabagh, M.M. Emara, Mg–Zn–Al LDH: influence of intercalated anions on CO₂ removal from natural gas, *Appl. Clay Sci.*, 160 (2018) 263–269.
- [31] J. Ni, J.J. Xue, L.F. Xie, J.Y. Shen, G.Y. He, H.Q. Chen, Construction of magnetically separable NiAl LDH/Fe₃O₄-RGO nanocomposites with enhanced photocatalytic performance under visible light, *Phys. Chem. Chem. Phys.*, 20 (2017) 414–421.
- [32] D. Chen, X.B. Wang, X.L. Wang, K. Feng, J.C. Su, J.N. Dong, The mechanism of cadmium sorption by sulphur-modified wheat straw biochar and its application cadmium-contaminated soil, *Sci. Total Environ.*, 714 (2020) 136550, doi: 10.1016/j.scitotenv.2020.136550.
- [33] X. Zhang, Y. Xue, J. Gao, C. He, Y. Ji, Y. Dou, Comparison of adsorption mechanisms for cadmium removal by modified zeolites and sands coated with Zn-layered double hydroxides, *Chem. Eng. J.*, 380 (2020) 122578, doi: 10.1016/j.cej.2019.122578.
- [34] H. Hu, S. Wageh, A.A. Al-Ghamdi, S. Yang, Z. Tian, B. Cheng, W. Ho, NiFe-LDH nanosheet/carbon fiber nanocomposite with enhanced anionic dye adsorption performance, *Appl. Surf. Sci.*, 511 (2020), doi: 10.1016/j.apsusc.2020.145570.
- [35] G.D. Vuković, A.D. Marinković, M. Čolić, M.D. Ristić, R. Aleksić, A.A. Perić-Grujić, P.S. Uskoković, Removal of cadmium from aqueous solutions by oxidized and ethylenediamine-functionalized multi-walled carbon nanotubes, *Chem. Eng. J.*, 157 (2010) 238–248.
- [36] M. Dinaria, A. Haghghia, P. Asadi, Facile synthesis of ZnAl-EDTA layered double hydroxide/poly(vinyl alcohol)

- nanocomposites as an efficient adsorbent of Cd(II) ions from the aqueous solution, *Appl. Clay Sci.*, 170 (2019) 21–28.
- [37] J.Q. Deng, Y.Q. Liu, S.B. Liu, G.M. Zeng, X.F. Tan, B.Y. Huang, Z.L. Yan, Competitive adsorption of Pb(II), Cd(II) and Cu(II) onto chitosan-pyromellitic dianhydride modified biochar, *J. Colloid Interface Sci.*, 506 (2017) 355–364.
- [38] L.S. Kostenko, I.I. Tomashchuk, T.V. Kovalchuk, O.A. Zaporozhets, Bentonites with grafted aminogroups: synthesis, protolytic properties and assessing Cu(II), Cd(II) and Pb(II) adsorption capacity, *Appl. Clay Sci.*, 172 (2019) 49–56.
- [39] L.G. Yan, S. Li, H.Q. Yu, R.R. Shan, B. Du, T.T. Liu, Facile solvothermal synthesis of Fe₃O₄/bentonite for efficient removal of heavy metals from aqueous solution, *Powder Technol.*, 301 (2016) 632–640.
- [40] X.R. Huang, H.H. Zhao, G.B. Zhang, J.T. Li, Y. Yang, P.H. Ji, Potential of removing Cd(II) and Pb(II) from contaminated water using a newly modified fly ash, *Chemosphere*, 242 (2020) 125148, doi: 10.1016/j.chemosphere.2019.125148.
- [41] B.D. Wang, Y.X. Zhou, L. Li, H. Xu, Y.L. Sun, Y. Wang, Novel synthesis of cyano-functionalized mesoporous silica nanospheres (MSN) from coal fly ash for removal of toxic metals from wastewater, *J. Hazard. Mater.*, 345 (2018) 76–86.
- [42] K.C. Justi, V.T. Fávère, M.C.M. Laranjeira, A. Neves, R.A. Peralta, Kinetics and equilibrium adsorption of Cu(II), Cd(II), and Ni(II) ions by chitosan functionalized with 2[-bis-(pyridylmethyl)aminomethyl]-4-methyl-6-formylphenol, *J. Colloid Interface Sci.*, 291 (2005) 369–374.
- [43] W.Y. Huang, D. Li, Z.Q. Liu, Q. Tao, Y. Zhu, J. Yang, Y.M. Zhan, Kinetics, isotherm, thermodynamic, and adsorption mechanism studies of La(OH)₃-modified exfoliated vermiculites as highly efficient phosphate adsorbents, *Chem. Eng. J.*, 236 (2014) 191–201.
- [44] A. Sharma, B.K. Lee, Cd(II) removal and recovery enhancement by using acrylamide-titanium nanocomposite as an adsorbent, *Appl. Surf. Sci.*, 313 (2014) 624–632.
- [45] H.G. Zhou, Z.M. Jiang, S.Q. Wei, A new hydrotalcite-like adsorbent FeMnMg-LDH and its adsorption capacity for Pb²⁺ ions in water, *Appl. Clay Sci.*, 153 (2018) 29–37.